

Perforation threshold energy of carbon fiber composite laminates

Shun-Fa Hwang*¹, Jia-Ching Li¹ and Ching-Ping Mao²

¹Department of Mechanical Engineering, National Yunlin University of Science and Technology,
123 University Road, Sec. 3, Douliu, Yunlin 64002, Taiwan, ROC

²Automotive Research & Testing Center, 6 Lugong S. 7th Road, Lugang, Changhua 50544, Taiwan, ROC

(Received March 19, 2011, Revised March 6, 2012, Accepted June 1, 2012)

Abstract. Two carbon fiber composite laminates, $[0/90]_{2S}$ and $[0/+45/90/-45]_S$, were considered in this work to find out the perforation threshold energy to complete the perforation process and the corresponding maximum contact force. Explicit finite element commercial software, LS-DYNA, was used to predict these values. According to the simulation results, these two types of composite laminates were tested by using a vertical drop-weight testing machine. After testing, the damage condition of these specimens were observed and compared with the results from finite element analysis. The testing results indicate that the perforation threshold energy is 6 Joules for $[0/90]_{2S}$ and 7 Joules for $[0/+45/90/-45]_S$, which is in good agreement with the simulation results. Also, the maximum contact force at the case of perforation threshold energy is the lowest as compared to the maximum contact forces occurring at the impact energy that is larger or less than the perforation threshold energy.

Keywords: composite; impact; finite element analysis; perforation threshold energy; contact force

1. Introduction

Composite materials have the characteristics of high modulus/weight and strength/weight ratios, excellent fatigue properties, and noncorroding behavior especially for polymer matrices. These advantages encourage the extensive applications of composites, for example, in marine, automobile, sports and aerospace. However, since there is generally no reinforcement in the thickness direction, composite laminates are susceptible to impact loading that may cause damage in the laminates. Impact loading may come from the drop of tools, the strike of birds, hails, or debris, secondary blast for offshore and industrial installations.

To predict the threshold of impact damage and the initiation of delaminations, Aslan *et al.* (2003) experimentally and numerically evaluated the in-plane dimensional effect of cross-ply E-glass/epoxy laminates under low-velocity impact. Meo *et al.* (2003) used LS-DYNA3D finite element code to predict the dent depth and the damage area of a composite aircraft sandwich panel under low-velocity impact and verified them by experiments. Jiang and Shu (2001) investigated the stress and damage in composite laminates subjected to transverse impact by a 3D finite element analysis and

*Corresponding author, Professor, E-mail: hwangsf@yuntech.edu.tw

concluded that the resistance of composite laminates to impact could be improved significantly by increasing the damage threshold. Nguyen *et al.* (2005) showed that an explicit finite element base simulation tool was capable of accurately predicting both the size and depth of the permanent indentation of sandwich structures and providing excellent correlation with the force-time histories. Duan *et al.* (2006) applied LS-DYNA to simulate the transverse impact of a right circular cylinder on a single layer plain-woven Kevlar fabric. When the impact velocity was high and caused the yarns to break instantaneously, the fabric failed along the periphery of the impact zone and the fabric boundary condition had no effect. Wang *et al.* (2006) utilized a finite element code to describe numerically the impact behavior of multi-layer multi-material printed circuit boards.

Because of their lamination structure, composite laminates have very complicated damage caused by penetration and perforation, which may include matrix cracking, fiber breakage, fiber pullout, surface micro-buckling, fiber matrix debonding, and delamination. Hashin's failure criterion was employed in damage assessment of bird impact on an airliner inboard flap structure by using highly detailed finite element models (Smojver and Ivancevic 2011), while qualitative correlation between numerical model and experimental test was obtained in terms of global deformation modes (Guida *et al.* 2011). As pointed out by Sun and Potti (1995), it would be a difficult task to model in detail the damage progression during penetration and perforation. Instead, the energy absorption mechanisms such as fiber damage, matrix damage, delamination and friction were identified (Zee and Hsieh 1993). This energy approach could give the basis for improving the perforation performance of the composites, for example, by using through-stitching to resist delamination (Lui 1990), a toughened resin system (Goldsmith *et al.* 1995), ductile fibers (Lee *et al.* 1994), or assembled composite plates that assemble multiple thin composite plates (Liu *et al.* 2000). Liu *et al.* (1998) pointed out that perforation is the most important damage stage in composite laminates subjected to impact loading because impact characteristics and mechanical properties degradation of composite laminates reach critical values when perforation takes place. The penetration and perforation of fiber-reinforced plastic laminates struck by rigid projectiles with different nose shapes using ABAQUS/Explicit code were examined (He *et al.* 2007, 2008) and the depth of penetration, ballistic limit, and velocity and deceleration of the projectile were obtained. Projectile nose angle effects in ballistic perforation of high strength fabric were analyzed by LS-DYNA code (Talebi *et al.* 2009). Dean *et al.* (2011) indicated that, with increasing impact velocity, the absorbed energy during projectile penetration of thin, lightweight sandwich panels with metallic fiber cores decreased from the ballistic limit, reached a minimum value, and then underwent a monotonic increase. Atas *et al.* (2011) presented an experimental investigation on the impact response of repaired and unrepaired glass/epoxy composite plates and revealed that perforation threshold energy of the repaired samples was around 120 J while that of intact samples was larger than 150 J.

The purpose of this work is to find out the perforation threshold energy and the corresponding maximum contact force for composite laminates by a numerical method and experiments. The perforation threshold energy means the impact energy required to just complete the perforation process. Two carbon fiber composite laminates, $[0/90]_{2s}$ and $[0/+45/90/-45]_s$, were considered in this work. Explicit finite element commercial software, ANSYS/LS-DYNA, was used to predict their perforation threshold energy and contact force. According to the simulation results, these two types of composite laminates were tested by a vertical drop-weight testing machine. After testing, the damage condition of these specimens was observed and compared with the results of finite element analysis.

2. Experimental details

To measure the mechanical properties of the composite laminates, three types of uniaxial tensile testing and two types of compression testing were executed. For tensile testing, two types of specimens, $[0]_8$ and $[90]_8$, were tested according to ASTM D3039, and $[\pm 45]_{4S}$ specimens were tested according to ASTM D3518. For compression testing, $[0]_{16}$ specimens with the dimension of $85 \times 12.7 \times 2$ mm and $[90]_{16}$ specimens with the dimension of $85 \times 25.2 \times 2$ mm were tested to obtain the longitudinal and transverse compression properties. The measured mechanical properties of the composite are listed in Table 1, in which the indicial notation is used. The longitudinal direction is denoted as 1 and the transverse direction is referred to as 2. The Young's modulus is represented as E , the Poisson's ratio as ν , and the shear modulus as G . Also, ρ is the density, S is the shear strength and X represents the other strengths. The subscript t denotes tensile and c represents compression.

As for the impact testing, two types of specimens, $[0/90]_{2S}$ and $[0/+45/90/-45]_S$, were considered, and their dimensions were $120 \times 120 \times 1$ mm. The impact was executed in a CEAST drop-weight testing system, and the specimen was under circular clamped support such that only the central circular area with 72 mm diameter was left for the impact. The hemispherical projectile had the diameter of 12 mm and the length of 32 mm. To impact the target, the projectile was released from the preset height and dropped freely according to the gravitational force. Once impact began, the contact forces were detected by the force transducer attached to the projectile and recorded in a computer. The impact energy could be adjusted according to the present height of the crosshead. To have the impact energies of 5, 6, and 7 J, the projectile with the mass of 1.063 kg was released from the heights of 0.38, 0.575, and 0.67 m, respectively. The projectile with the mass of 1.262 kg was released from 0.645 m height to create the impact energy of 8 J. After impacting, the damage of the specimen was observed.

To fabricate the above composite laminates, the bag molding process was used. The prepreg that consists of unidirectional 12 K carbon fiber with 125 g/m^2 and 37 wt. % resin was supplied by Wah Lee Corp. After the prepreg was bagged, it was vacuumed and placed on a hot press. A two-stage cure cycle was executed. In the first stage temperature was increased at a controlled rate up to 80°C without any application of pressure and was held for 30 min. In the second stage, temperature was

Table 1 Mechanical properties of the composite

Property	Magnitude
ρ	$1.5\text{E-}6 \text{ kg/mm}^3$
E_{11}	135.8 GPa
E_{22}	7.61 GPa
G_{12}	4.59 GPa
ν_{12}	0.2
S	102 MPa
X_{1t}	1785 MPa
X_{2t}	42.5 MPa
X_{1c}	739 MPa
X_{2c}	158 MPa

increased to 120°C and a pressure around 2.07-2.62 MPa was applied. Then, the temperature and pressure were maintained for one hour. At the end of the cure cycle, the temperature was slowly reduced while the laminate was still under pressure.

3. Numerical simulation

To predict the perforation threshold energy, an explicit commercial finite element code, LS-DYNA, was used to simulate the impact process of the two types of composite laminates. The projectile was assumed to be a rigid body and the composite laminate was treated as an orthotropic elastic material. Both the projectile and the laminates were meshed by shell elements, SHELL163, which were 4-node elements with bending and membrane capabilities. In this element, the Hughes-Liu element formulation was chosen and one-point quadrature was used with the control of hourglassing. Since there were 8 layers in the laminate, each layer along the thickness direction was assigned one-point quadrature in the integration scheme. The projectile with the velocity that was calculated from the impact energy was put at 1.5 mm above the surface of the laminate. In addition, the adaptive function to automatically and locally increase the mesh density was triggered. Totally, there were about 10078 nodes and 7822 elements in the simulation as shown in Fig. 1. To be compatible with the experiment, the dimension of the whole specimen was 120 × 120 × 1 mm, and the bottom surface of the specimen outside of the central circular area with 72 mm diameter was fixed in the simulation. Lagrangian formulation was selected because it is generally appropriate for impact of solid bodies. Both the temperature effect and the strain rate effect were not considered in this simulation because the impact velocities were very low.

A phenomenological criterion proposed by Hashin (1980) was used to describe the failure behavior of the laminates. Hashin's failure law for plane stress condition can be described as the follows.

Longitudinal tensile failure

$$\left\{ \frac{\sigma_{11}}{X_{1t}} \right\}^2 + \left\{ \frac{\sigma_{12}}{S} \right\} = 1 \quad (1)$$

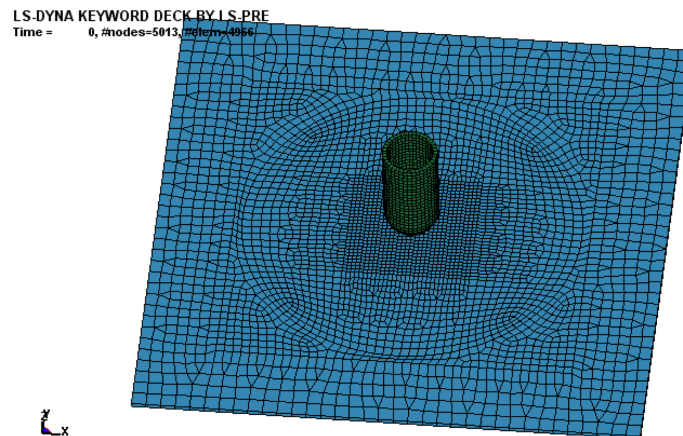


Fig. 1 Finite element mesh

Longitudinal compression failure

$$\left\{ \frac{\sigma_{11}}{X_{1c}} \right\}^2 = 1 \tag{2}$$

Transverse tensile failure

$$\left\{ \frac{\sigma_{22}}{X_{2t}} \right\}^2 + \left\{ \frac{\sigma_{12}}{S} \right\} = 1 \tag{3}$$

Transverse compression failure

$$\left(\frac{\sigma_{22}}{2S} \right)^2 + \left[\left(\frac{X_{2c}}{2S} \right)^2 - 1 \right] \frac{\sigma_{22}}{X_{2c}} + \left(\frac{\sigma_{12}}{S} \right)^2 = 1 \tag{4}$$

where σ represents the applied stress and the indicial notation is used.

4. Results and discussion

4.1 [0/+45/90/-45]_S specimens

After some trials in the finite element simulation, it is found that the perforation threshold energy of [0/+45/90/-45]_S specimens is around 6 to 8 J, and these energies are considered as the impact energy. During the simulation, the total energy is observed to check if there is any hourglassing noticeable. Fig. 2 shows the energies during the impact process for impact energy of 6 J. It demonstrates that there is no hourglassing in the present simulation because the total energy could be kept constant during the impact process. For the three impact energies, the simulation results are shown in Figs. 3-5. Fig. 3 illustrates that the projectile with 6 J still does not perforate the composite laminate, and when the projectile has the kinetic energy of 8 J, it has perforated the laminate as shown in Fig. 5. Hence, the critical situation should be around 7 J as shown in Fig. 4. These three impact energies were also applied in the impact testing, and the testing conditions as

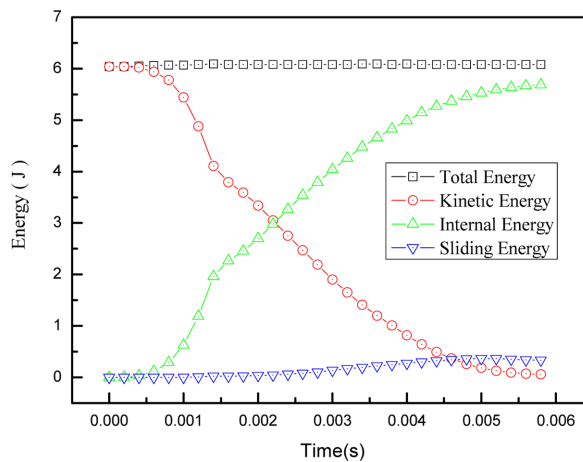


Fig. 2 Energies during the impact process under 6 J for [0/+45/90/-45]_S

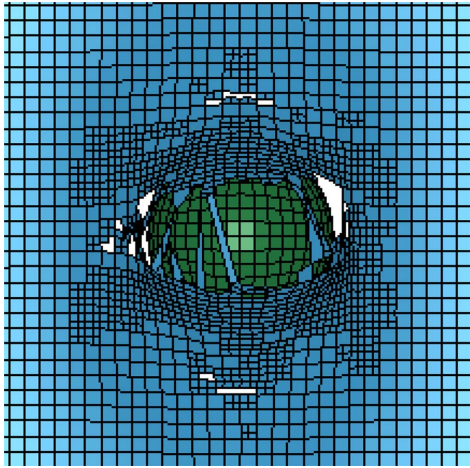


Fig. 3 Zoom view of the damaged area under the impact energy of 6 J for $[0/+45/90/-45]_s$

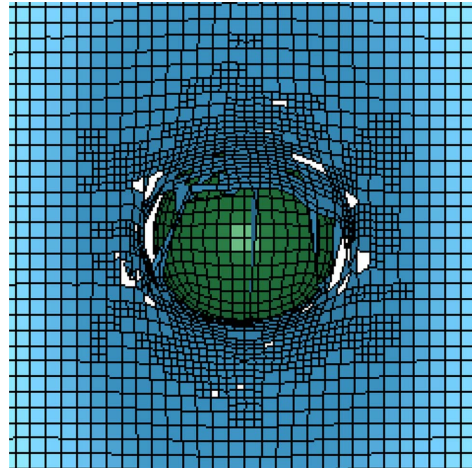


Fig. 4 Zoom view of the damaged area under the impact energy of 7 J for $[0/+45/90/-45]_s$

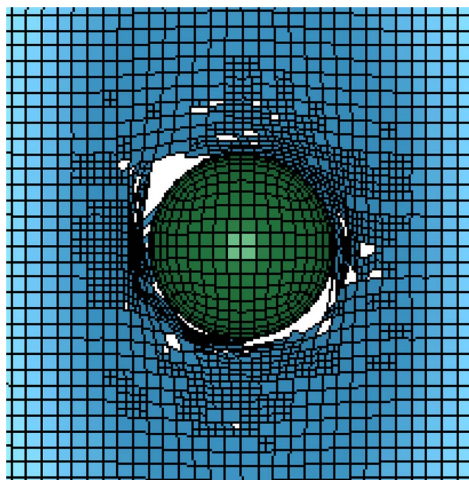


Fig. 5 Zoom view of the damaged area under the impact energy of 8 J for $[0/+45/90/-45]_s$

well as the measured maximum contact forces are listed in Table 2. The damaged areas caused by these three impact energies are shown in Figs. 6-8. These testing results confirm the simulation results that the impact energy of 7 J should be the perforation threshold energy. As shown in these figures, the damaged area observed from the top side of the specimen is a circle, and it is increased with the impact energy.

When the contact force during the impact process under 6 J is considered, the simulation result is shown in Fig. 9 and the maximum contact force is 1350 N. For the cases of 7 and 8 J, the maximum contact force is 1295 and 1592 N, respectively. It is surprising to find out that the impact energy of 7 J has the lowest maximum contact force as compared to the other two impact energies. From the experimental testing results as shown in Table 2, this situation is also verified. For example, the average maximum contact force is 1373, 1320, and 1405 N for the impact energy of 6,

Table 2 Impact testing results for $[0/+45/90/-45]_s$

Specimen	Energy (J)	Mass (kg)	Height (m)	Velocity (m/s)	Force (N)
1	6	1.063	0.575	3.358	1406.24
2	6	1.063	0.575	3.358	1302.72
3	6	1.063	0.575	3.358	1410.56
Average					1373.17
4	7	1.063	0.67	3.62	1315.66
5	7	1.063	0.67	3.62	1419.18
6	7	1.063	0.67	3.62	1225.07
Average					1319.97
7	8	1.263	0.645	3.557	1492.52
8	8	1.263	0.645	3.557	1367.42
9	8	1.263	0.645	3.557	1354.48
Average					1404.80

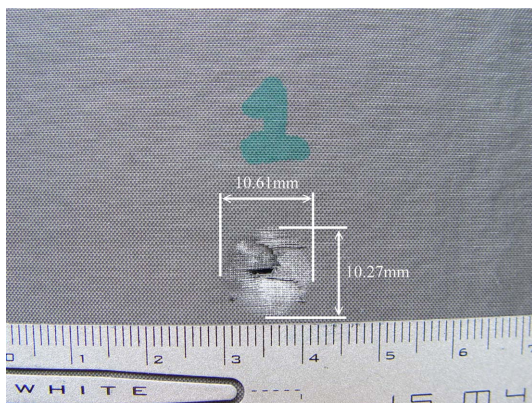


Fig. 6 Damaged area of impact testing under 6 J for $[0/+45/90/-45]_s$

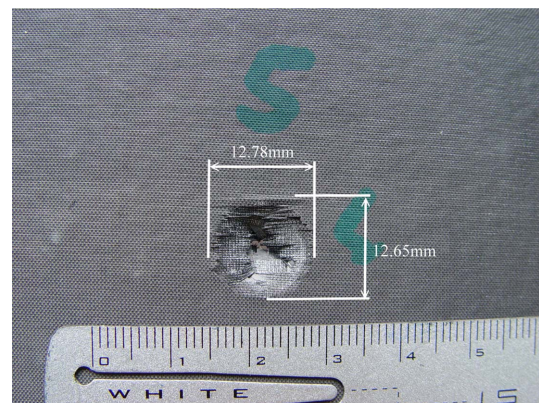


Fig. 7 Damaged area of impact testing under 7 J for $[0/+45/90/-45]_s$

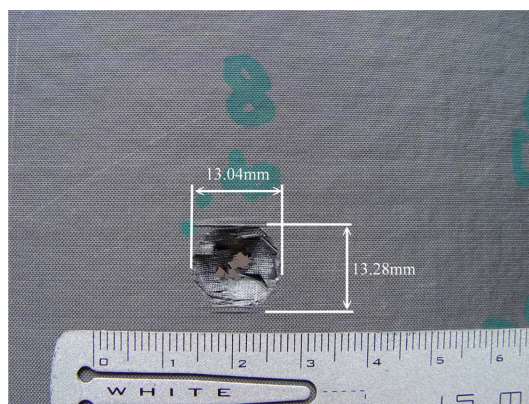


Fig. 8 Damaged area of impact testing under 8 J for $[0/+45/90/-45]_s$

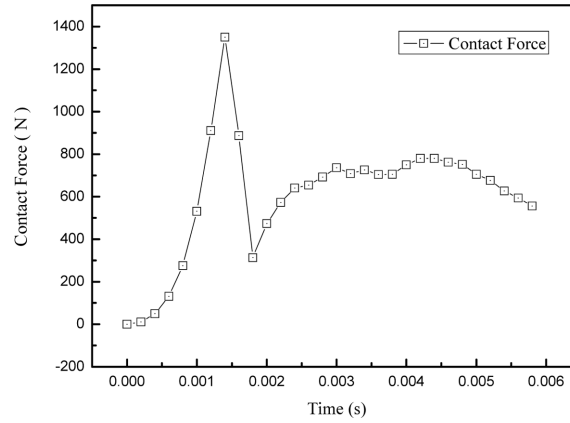


Fig. 9 Simulation contact force during the impact process under 6 J for $[0/+45/90/-45]_s$

7, and 8 J, respectively. One possible explanation to this lowest maximum contact force occurred on the case of perforation threshold energy is the long contact time during the impact process as compared to the other two cases. By the way, the difference between the simulation and the experiment on the maximum contact force is below 2% for the first two cases, while it is around 13% for the third case. From Table 2, the measured maximum contact forces for the three repeated impact testing present about 8% to 15% variation among themselves or about 5% to 8% variation as compared to their average value. According to this, the above 2% to 13% difference between the simulation and the experiment should be reasonable.

4.2 $[0/90]_{2s}$ specimens

For this type of specimens, the considered impact energies are 5, 6, 7 J. The simulation results are illustrated in Figs. 10-12 and the testing results are shown in Table 3 and Figs. 13-15. From

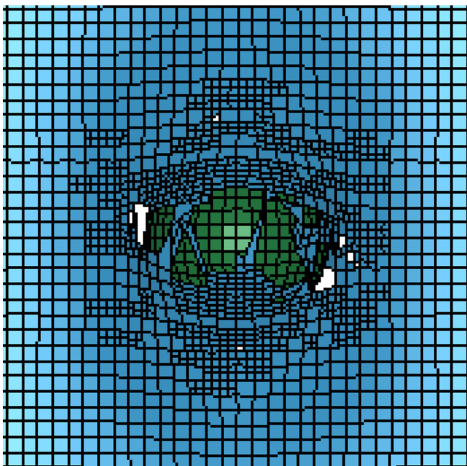


Fig. 10 Zoom view of the damaged area under the impact energy of 5 J for $[0/90]_{2s}$

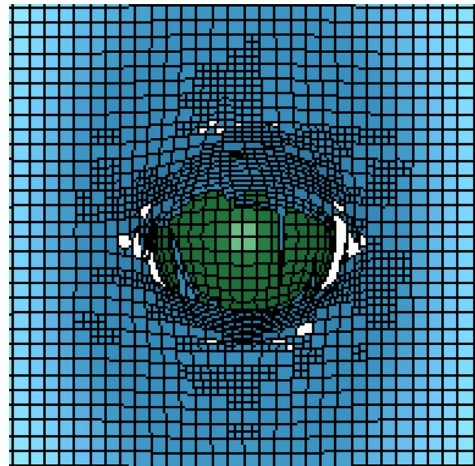
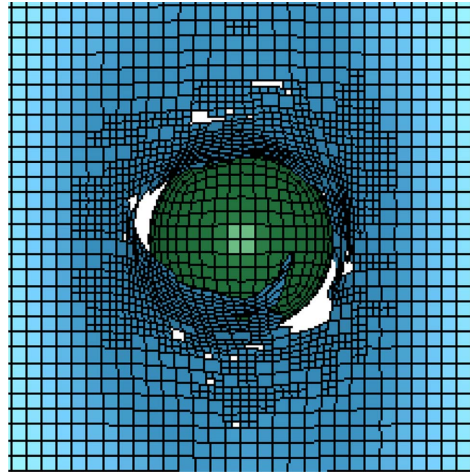


Fig. 11 Zoom view of the damaged area under the impact energy of 6 J for $[0/90]_{2s}$

Fig. 12 Zoom view of the damaged area under the impact energy of 7 J for $[0/90]_{2S}$ Table 3 Impact testing results for $[0/90]_{2S}$

Specimen	Energy (J)	Mass (kg)	Height (m)	Velocity (m/s)	Force (N)
1	5	1.063	0.48	3.06	1419.18
2	5	1.063	0.48	3.06	1367.42
3	5	1.063	0.48	3.06	1462.32
Average					1416.03
4	6	1.063	0.575	3.358	1466.63
5	6	1.063	0.575	3.358	1384.68
6	6	1.063	0.575	3.358	1242.33
Average					1364.54
7	7	1.063	0.67	3.62	1604.67
8	7	1.063	0.67	3.62	1544.28
9	7	1.063	0.67	3.62	1509.77
Average					1552.90

these results, the perforation threshold energy of $[0/90]_{2S}$ specimens should be 6 Joules. According to the simulation, the maximum contact force during the impact process is 1499, 1356, and 1647 N for 5, 6, and 7 J, respectively. The average maximum contact forces measured from impact testing are 1416, 1365, and 1553 N for 5, 6, and 7 J, respectively. The difference between the simulation and the experiment is less than the variation between the three repeated impact testing, and the prediction from the simulation should be reasonable. Similarly, the case with the perforation threshold energy has the lowest maximum contact force. As comparing the two types of composite laminates, $[0/+45/90/-45]_S$ specimens have higher perforation threshold energy and lower maximum contact force. This effect may result from the presence of the $[\pm 45]$ layers. That is to say, the quasi-isotropic composite laminates have higher resistance to the perforation as compared to their cross-ply counterparts.

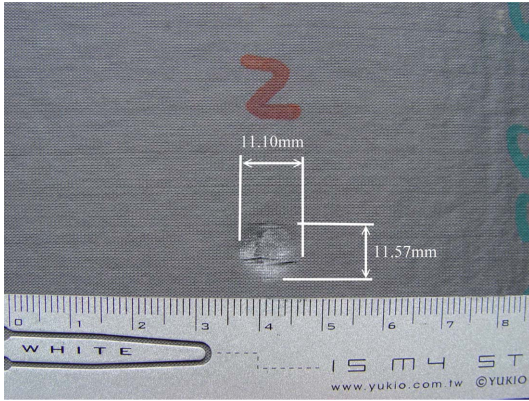


Fig. 13 Damaged area of impact testing under 5 J for $[0/90]_{2S}$

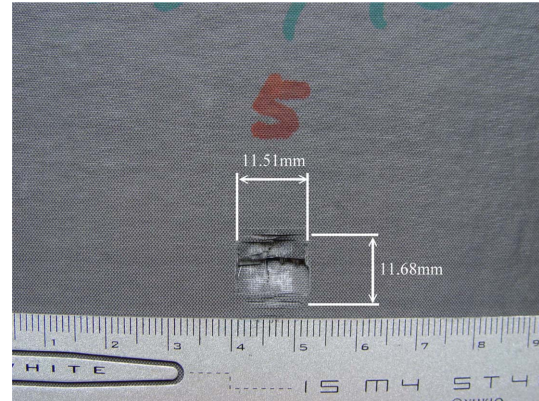


Fig. 14 Damaged area of impact testing under 6 J for $[0/90]_{2S}$

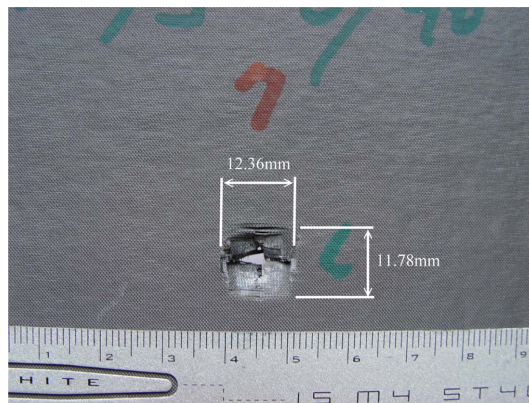


Fig. 15 Damaged area of impact testing under 7 J for $[0/90]_{2S}$

5. Conclusions

Two carbon fiber composite laminates, $[0/90]_{2S}$ and $[0/+45/90/-45]_S$, were considered in this work to find out the perforation threshold energy to complete the perforation process and the corresponding maximum contact force. Explicit finite element commercial software, LS-DYNA, was used to predict these values. Vertical drop-weight impact tests were executed to confirm the simulation. The simulation indicates that the perforation threshold energy is 7 J for $[0/+45/90/-45]_S$ and 6 J for $[0/90]_{2S}$, which are confirmed by the impact testing. The predicted maximum contact forces are in reasonable agreement with the average maximum contact forces from impact testing. It is surprising to find out that the maximum contact force at the case of perforation threshold energy is the lowest as compared to the maximum contact forces occurring at the impact energy that is larger or less than the perforation threshold energy. As comparing the two types of composite laminates, $[0/+45/90/-45]_S$ specimens have higher perforation threshold energy and lower maximum contact force. This effect may result from the presence of the $[\pm 45]$ layers. That is to say, the quasi-

isotropic composite laminates have higher resistance to the perforation as compared to their cross-ply counterparts.

References

- Aslan, Z., Karakuzu, R. and Okutan, B. (2003), "The response of laminated composite plates under low-velocity impact loading", *Compos. Struct.*, **59**, 119-127.
- Atas, C. Akgun, Y., Dagdelen, O., Icten, B.M. and Sarikanat, M. (2011), "An experimental investigation on the low velocity impact response of composite plates repaired by VARIM and hand lay-up processes", *Compos. Struct.*, **93**, 1178-1186.
- Dean, J., S-Fallah, A., Brown, P.M., Louca, L.A. and Clyne, T.W. (2011), "Energy absorption during projectile perforation of lightweight sandwich panels with metallic fibre cores", *Compos. Struct.*, **93**, 1089-1095.
- Duan, Y., Keefe, M., Bogetti, T.A. and Powers, B. (2006), "Finite element modeling of transverse impact on a ballistic fabric", *Int. J. Mech. Sci.*, **48**, 33-43.
- Goldsmith, W., Dharan, C.K.H. and Chang, H. (1995), "Quasi-static and ballistic perforation of carbon fibre laminates", *Int. J. Solid Struct.*, **32**, 89-103.
- Guida, M., Marulo, F., Meo, M., Grimaldi, A. and Olivares, G. (2011), "SPH – Lagrangian study of bird impact on leading edge wing", *Compos. Struct.*, **93**, 1060-1071.
- Hashin, Z. (1980), "Failure criteria for unidirectional fiber composites", *J. Appl. Mech.*, **47**, 329-334.
- He, T., Wen, H.M. and Qin, Y. (2007), "Penetration and perforation of FRP laminates struck transversely by conical-nosed projectiles", *Compos. Struct.*, **81**, 243-252.
- He, T., Wen, H.M. and Qin, Y. (2008), "Finite element analysis to predict penetration and perforation of thick FRP laminates struck by projectiles", *Int. J. Impact Eng.*, **35**, 27-36.
- Jiang, D. and Shu, D. (2001), "Effects of damage threshold on stresses in composite laminates under transverse impact", *Compos. Struct.*, **66**, 61-67.
- Lee, B.L., Song, J.W. and Ward, J.E. (1994), "Fibre reinforced composites under ballistic impact loading", *J. Compos. Mater.*, **28**, 1202-1226.
- Liu, D. (1990), "Delamination resistance in stitched and unstitched composite plates subjected to impact loading", *J. Reinf. Plast. Compos.*, **9**, 59-69.
- Liu, D., Basavaraju, B.R. and Dang, X. (2000), "Impact perforation resistance of laminated and assembled composite plates", *Int. J. Impact Eng.*, **24**, 733-746.
- Liu, D., Raju, B.B. and Dang, X. (1998), "Size effects on impact response of composite laminates", *Int. J. Impact Eng.*, **21**, 837-854.
- Meo, M., Morris, A.J., Vignjevic, R. and Marengo, G. (2003), "Numerical simulation of low-velocity impact on an aircraft sandwich panel", *Compos. Struct.*, **62**, 353-360.
- Nguyen, M.Q., Jacombs, S.S., Thomson, R.S., Hachenberg, D. and Scott, M.L. (2005), "Simulation of impact on sandwich structures", *Compos. Struct.*, **67**, 217-227.
- Smojver, I. and Ivancevic, D. (2011), "Bird strike damage analysis in aircraft structures using Abaqus/explicit and coupled Eulerian Lagrangian approach", *Compos. Sci. Tech.*, **71**, 489-498.
- Sun, C.T. and Potti, S.V. (1995), "Modeling dynamic penetration of thick section composite laminates", *Proceedings of the 36th AIAA/ASME/ASCE/AHS/ASC SDM Conference and AIAA/ASME Adaptive Structures Forum*, New Orleans, Louisiana.
- Talebi, H., Wong, S.V. and Hamouda, A.M.S. (2009), "Finite element evaluation of projectile nose angle effects in ballistic perforation of high strength fabric", *Compos. Struct.*, **87**, 314-320.
- Wang, Y., Low, K.H., Pang, H.L.J., Hoon, K.H., Che, F.X. and Yong, Y.S. (2006), "Modeling and simulation for a drop-impact analysis of multi-layered printed circuit boards", *Microelectron Reliab.*, **46**, 558-573.
- Zee, R.H. and Hsieh, C.Y. (1993), "Energy loss partitioning during ballistic impact of polymer composites", *Polym. Compos.*, **14**, 265-271.